

# Non-oxidative decomposition of methanol into hydrogen in a rotating gliding arc plasma reactor

Hao Zhang<sup>a, b</sup>, Xiaodong Li<sup>a, \*</sup>, Fengsen Zhu<sup>a</sup>, Zheng Bo<sup>a</sup>, Kefa Cen<sup>a</sup>, Xin Tu<sup>b, \*</sup>

<sup>a</sup> State Key Laboratory of Clean Energy Utilization, Zhejiang University, 38# Zheda Road, Hangzhou, Zhejiang 310027, China

<sup>b</sup> Department of Electrical Engineering and Electronics, University of Liverpool, Brownlow Hill, Liverpool L69 3GJ, UK

## ABSTRACT

A direct current rotating gliding arc (RGA) reactor co-driven by a magnetic field and tangential flow has been developed for the non-oxidative decomposition of methanol into hydrogen and other valuable products. The influence of input CH<sub>3</sub>OH concentration and carrier gas (N<sub>2</sub> and Ar) on the reaction performance of the plasma process has been investigated in terms of the conversion of methanol, product selectivity, and energy efficiency of the process. The maximum CH<sub>3</sub>OH conversion of 92.4% and hydrogen selectivity of 53.1% are achieved in the plasma methanol conversion using N<sub>2</sub> as a carrier gas. Optical emission diagnostics has shown the formation of a variety of reactive species (e.g., H, OH, CH, CN, N<sub>2</sub> and C<sub>2</sub>) in the plasma decomposition of methanol. The vibrational and electronically excited species (e.g., N<sub>2</sub> (A<sup>3</sup>Σ<sub>u</sub><sup>+</sup>) and Ar\*) could be critical in the conversion of CH<sub>3</sub>OH, leading to a higher CH<sub>3</sub>OH conversion in the CH<sub>3</sub>OH/N<sub>2</sub> RGA due to the presence of more reaction pathways. Compared to other non-thermal plasmas, the RGA plasma shows a much better process performance, offering a promising and flexible route for hydrogen production.

**Keywords:** Rotating gliding arc; Methanol decomposition; Hydrogen production; Optical emission

---

\* Corresponding author. Tel.: +86-571-87952037 (X. D. Li); +44-1517944513 (X. Tu)  
E-mail address: [lixd@zju.edu.cn](mailto:lixd@zju.edu.cn) (X. D. Li); [xin.tu@liv.ac.uk](mailto:xin.tu@liv.ac.uk) (X. Tu)

spectroscopy; Reaction mechanisms

## 1. Introduction

Recently, the development of novel and cost-effective hydrogen production processes has attracted significant interest due to the depletion of fossil fuels and [the environmental impact of the usage of fossil fuels](#). However, technical problems with the handling, storage, and transport of hydrogen largely limit its widespread use, particularly in portable fuel cells which have been considered as a promising alternative to the traditional battery technology [1]. The development of portable hydrogen generation systems could provide a source of clean hydrogen for portable fuel cells [2]. Methanol has been considered as an excellent H<sub>2</sub>-containing source for portable hydrogen production due to its high hydrogen to carbon ratio, easy transportation, and low boiling point [3-8]. Catalytic steam reforming of methanol has been extensively investigated for hydrogen production [9]. However, this process still faces technical challenges that limit [its use](#) in a commercial-scale system. Although significant efforts have been devoted to find active, stable, and cost-effective catalysts for producing hydrogen from methanol, rapid deactivation of catalysts and the requirement of high temperature in the reforming process [incur](#) high energy and operational costs and consequently [limit](#) its industrial applications, particularly in on-board hydrogen production systems [10].

Non-thermal plasma technology provides an attractive alternative to the conventional catalytic route for methanol conversion at a relatively low temperature [1-8, 11, 12]. In non-thermal plasmas, the overall gas temperature can be as low as room temperature, while the electrons are highly energetic, with a typical electron temperature of 1-10 eV, which is sufficient to break down most chemical bonds of gas molecules and produce chemically reactive species including the excited

atoms, ions and molecules for the initiation and propagation of chemical reactions [12]. High reaction rate and fast attainment of steady state in the plasma processes allows rapid start-up and shutdown of the plasma process, providing highly flexibility to be integrated into portable hydrogen production systems [11, 12]. Different non-thermal plasma systems have been developed for methanol conversion into hydrogen to maximize hydrogen production and energy efficiency of the plasma process, such as microhollow cathode discharge (MHCD) [2], microwave discharge [5-8], and dielectric barrier discharge (DBD) [13]. However, the relatively low power level of these plasma systems makes it difficult to achieve high, efficient conversion of methanol at a high gas flow rate, restricting the potential scale-up of this process [14]. For instance, Futamura et al. reported a methanol conversion of only 8-26% can be obtained at a feed N<sub>2</sub> flow rate of 100 ml/min and an input CH<sub>3</sub>OH concentration of 1% in the plasma decomposition of methanol using a DBD [15].

Gliding arc discharge (GAD) has been considered as a transitional plasma with a relatively high electron density and high flexibility to work in a wide range of reactant flow rates and plasma power levels (up to several kW) [11, 16-18]. In a traditional GAD reactor that consists of two divergent knife-shaped electrodes, high flow rate (e.g., 10-20 l/min) is generally required to push the arc moving along the electrodes, generating a discharge zone for chemical reactions. As a consequence, the fast gas speed and limited two-dimensional plasma reaction area confined by the flat electrodes lead to a low retention time of reactants, thereby limiting the conversions of reactants and the energy efficiency of the plasma process [14, 19].

A direct current (DC) rotating gliding arc (RGA) co-driven by a magnetic field and tangential flow has been developed for hydrogen production from methane conversion in our previous work [19]. Compared to the traditional gliding arc system with knife-shaped electrodes, the RGA reactor

can generate a synergetic effect resulting from the combination of swirling flow and Lorentz force, which can make the arc rotate rapidly and steadily without extinction (with a rotational speed of up to 100 rotations per second) with a wide range of gas flow rate (e.g., 0.05-40 l/min), creating a three-dimensional stable plasma area with the increased retention time of the reactants in plasma chemical reactions. Our previous study showed that this RGA system significantly improved the performance of plasma methane conversion with a maximum CH<sub>4</sub> conversion of 91.8%, a hydrogen selectivity of 80.7% and a maximum energy yield of H<sub>2</sub> of 22.6 g/kWh [19].

In this study, an RGA plasma reactor has been developed for the non-oxidative decomposition of methanol into hydrogen. N<sub>2</sub> and Ar have been commonly used as the carrier gases in the plasma processes for energy conversion and fuel production [2, 5, 20]. Significant efforts have been devoted to investigating the effect of different operating parameters (e.g., input power, flow rate, etc.) on the performance of plasma chemical reactions, whereas less attention has been paid to understand the role of different carrier gases in the plasma chemical processes. This is of primary importance because different carrier gases will generate different reactive species and significantly affect the plasma chemical reactions in different ways, especially the methanol decomposition process [19, 21]. In this work, the effect of input CH<sub>3</sub>OH concentration and carrier gas (N<sub>2</sub> and Ar) on the reaction performance (e.g., conversion of methanol, selectivity of gas products, and energy efficiency) of the methanol conversion process has been investigated in an RGA plasma reactor. Optical emission spectroscopy (OES) has been used to give new insights into the formation of reactive species in the plasma chemical reactions. In addition, the possible reaction pathways in the plasma methanol decomposition process using different carrier gases have been discussed. Finally, a comparison of the methanol conversion process using different plasma systems has been carried out.

## 2. Experimental

### 2.1 Experimental setup and gas analysis

Fig. 1 shows the schematic diagram of the experimental set-up. A con-shaped stainless steel electrode (anode) is placed inside a circular stainless steel cylinder which acts as a cathode. A more detailed description of the RGA reactor can be found in our previous work [19]. The carrier gas ( $N_2$  or Ar) was injected through three tangential inlets at the bottom of the reactor to form a swirling flow in the reactor. A magnet was placed outside the reactor to generate a magnetic field for the stabilization and acceleration of the arc. With the combined effect of swirling flow and Lorentz force, the arc moves upward and finally rotates rapidly around the inner electrode, forming a stable plasma volume for chemical reactions.

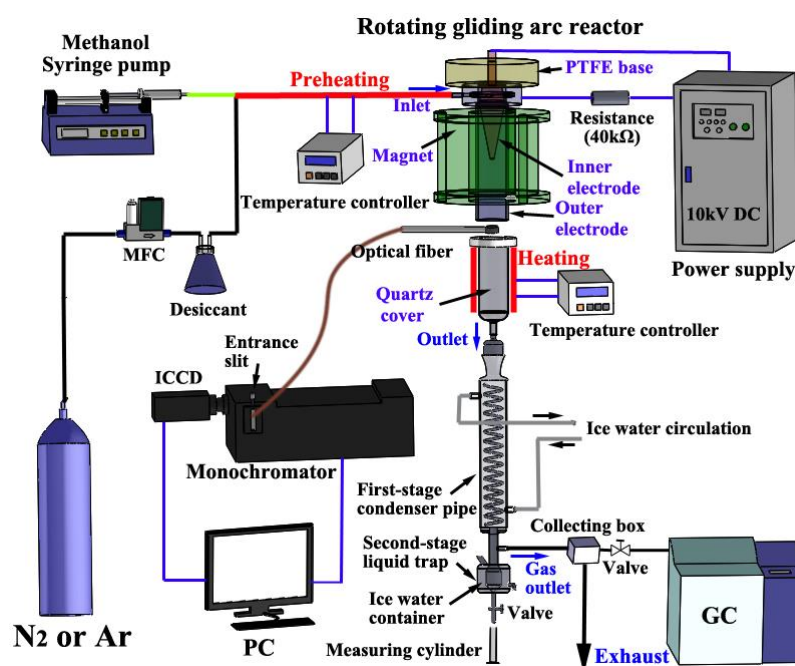


Fig. 1 – Schematic diagram of the experimental setup

Methanol was controlled and injected into the gas tube using a high-resolution syringe pump

(Harvard, 11 plus). In this way, the total feed flow rate (0.6 mol/min) of the mixed stream and input CH<sub>3</sub>OH concentration (5-35 mol %) could be controlled. The mixed stream was then heated to 100 °C in a stainless steel pipe with an inner diameter of 4 mm (40 cm in length) equipped with a temperature controller system, to generate a steady-state vapor before flowing into the RGA reactor. The quartz cover of the plasma reactor was also heated to 100 °C to prevent any vapor condensation on the inner wall of the reactor. The plasma reactor was connected to a DC power supply (380 V/10 kV) with a 40-kΩ resistance connected in the circuit to limit and stabilize the breakdown current. A two-stage condenser was placed at the exit of the plasma reactor to collect the condensable vapors in the effluent: the first-stage condenser pipe was equipped with an ice water circulation system, while the second-stage liquid trap was placed inside the ice water container.

The gaseous products were measured by a gas chromatography (GC9790A, Fuli Analytical Instrument) equipped with a thermal conductivity detector (TCD) for the detection of H<sub>2</sub>, O<sub>2</sub>, and N<sub>2</sub> and a flame ionization detector (FID) for the analysis of CO, CO<sub>2</sub>, and hydrocarbons. The condensed liquid was measured by a gas chromatography – mass spectrometry (JEOL, JMS-Q1050GC). We found the condensed liquid was mainly methanol with trace amounts of ethanol, propanol and ethylene glycol. Thus, the volume of the condensed liquid can be roughly regarded as the volume of the unreacted methanol after the plasma reaction [4, 6, 22-24]. The emission spectra of the plasmas were recorded by a 750-mm monochromator (PI-Acton 2750, grating: 1800 grooves/mm) equipped with an intensified charge-coupled device (ICCD, PI-MAX 2, 512×512 pixel). An optical fiber was placed at the exit of the RGA reactor to collect the plasma radiation.

## 2.2 Definition of parameters

For the plasma methanol decomposition process, the conversion of CH<sub>3</sub>OH is defined as:

$$X(\text{CH}_3\text{OH})(\%) = \frac{\text{moles of CH}_3\text{OH converted}}{\text{moles of CH}_3\text{OH input}} \times 100\% \quad (1)$$

The selectivities (*S*) of the products can be calculated:

$$S(\text{H}_2)(\%) = \frac{\text{moles of H}_2 \text{ produced}}{2 \times \text{moles of CH}_3\text{OH converted}} \times 100\% \quad (2)$$

$$S(\text{CO})(\%) = \frac{\text{moles of CO produced}}{\text{moles of CH}_3\text{OH converted}} \times 100\% \quad (3)$$

$$S(\text{CO}_2)(\%) = \frac{\text{moles of CO}_2 \text{ produced}}{\text{moles of CH}_3\text{OH converted}} \times 100\% \quad (4)$$

$$S(\text{C}_m\text{H}_n)(\%) = \frac{m \times \text{moles of C}_m\text{H}_n \text{ produced}}{\text{moles of CH}_3\text{OH converted}} \times 100\% \quad (5)$$

The energy yield of H<sub>2</sub> is defined as:

$$EY(\text{H}_2)(\text{g/kWh}) = \frac{\text{grams of H}_2 \text{ produced per min.}}{\text{power}(\text{W}) \times 60/3600000} \times 100\% \quad (6)$$

The energy conversion efficiency (*ECE*) of the process is calculated based on the change of the lower heating values (*LHV*) of the fuels before and after the reaction.

$$ECE(\%) = \frac{\sum p_i \times LHV_i}{\text{power}(\text{W}) \times 60/1000 + \text{moles of CH}_3\text{OH converted per min} \times LHV_{\text{CH}_3\text{OH}}} \times 100\% \quad (7)$$

Where *p<sub>i</sub>* refers to the moles of produced fuel *i* (*i*: H<sub>2</sub>, CO, CH<sub>4</sub>, C<sub>2</sub>H<sub>4</sub>, and C<sub>2</sub>H<sub>2</sub>) per minute.

(*LHV*<sub>H<sub>2</sub></sub> = 241.6 kJ/mol, *LHV*<sub>CO</sub> = 283.0 kJ/mol, *LHV*<sub>CH<sub>4</sub></sub> = 803.7 kJ/mol, *LHV*<sub>C<sub>2</sub>H<sub>4</sub></sub> = 1331.5 kJ/mol,

*LHV*<sub>C<sub>2</sub>H<sub>2</sub></sub> = 1265.376 kJ/mol, *LHV*<sub>CH<sub>3</sub>OH</sub> = 638.5 kJ/mol)

## 3. Results and discussion

### 3.1 Plasma decomposition of methanol

H<sub>2</sub> and CO were the major gaseous products in the non-oxidative decomposition of methanol using the RGA plasma, while trace amounts of CO<sub>2</sub>, CH<sub>4</sub>, C<sub>2</sub>H<sub>2</sub>, and C<sub>2</sub>H<sub>4</sub> (total selectivity: 1.1-3.8%) were also formed. C<sub>2</sub>H<sub>6</sub> was only detected with a selectivity of 0.5% in the conversion of 5% methanol using the argon RGA plasma. Note that C<sub>2</sub>H<sub>6</sub> was identified as the main C<sub>2</sub> hydrocarbons in plasma processing of hydrocarbons using dielectric barrier discharges [25, 26]. However, previous work has also shown the shift of the distribution of C<sub>2</sub> hydrocarbon from C<sub>2</sub>H<sub>6</sub> to C<sub>2</sub>H<sub>2</sub> and C<sub>2</sub>H<sub>4</sub> in the dry reforming of methane and carbon dioxide using an AC gliding arc plasma [11]. No C<sub>3</sub> or higher hydrocarbons gases were detected in this experiment. In the plasma partial oxidation or steam reforming of methanol, significant undesired gaseous byproducts were often generated with high selectivity, such as HCHO (45-60% selectivity) [27] and CO<sub>2</sub> (11.8-95% selectivity) [13, 24], the plasma non-oxidative methanol decomposition process using an RGA reactor could produce much cleaner gas products of which the syngas is the main one.

The effect of input CH<sub>3</sub>OH concentration on the discharge power of the CH<sub>3</sub>OH/N<sub>2</sub> and CH<sub>3</sub>OH/Ar RGA plasmas is shown in Fig. 2. As we can see, the discharge power (149.8-349.4 W) of the CH<sub>3</sub>OH/N<sub>2</sub> plasma is much higher than that of the CH<sub>3</sub>OH/Ar plasma (105.2-271.6 W) at the same CH<sub>3</sub>OH concentration. In both plasma chemical reactions, the discharge power initially increases with the increase of the input CH<sub>3</sub>OH concentration to 20%, over which the discharge power is saturated when further increasing the CH<sub>3</sub>OH concentration to 35%.

Fig. 3 shows the effect of input CH<sub>3</sub>OH concentration on the conversion of CH<sub>3</sub>OH. Increasing the CH<sub>3</sub>OH concentration leads to a significant decrease of the CH<sub>3</sub>OH conversion, even though the discharge power of the plasmas is initially increased with methanol concentration. The conversion of CH<sub>3</sub>OH is higher in the CH<sub>3</sub>OH/N<sub>2</sub> plasma than that in the CH<sub>3</sub>OH/Ar RGA at the same methanol concentration, since the higher discharge power is generated in the CH<sub>3</sub>OH/N<sub>2</sub> plasma



with more reaction pathways due to the formation of a variety of excited species such as vibrational excited  $N_2$  and electronically excited  $N_2$ .

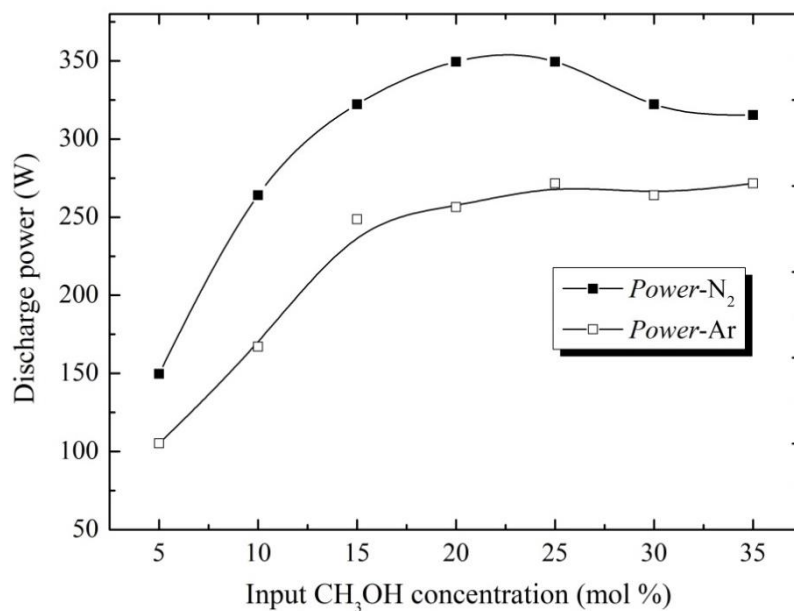


**Fig. 2 – Effect of input  $CH_3OH$  concentration on the discharge power**

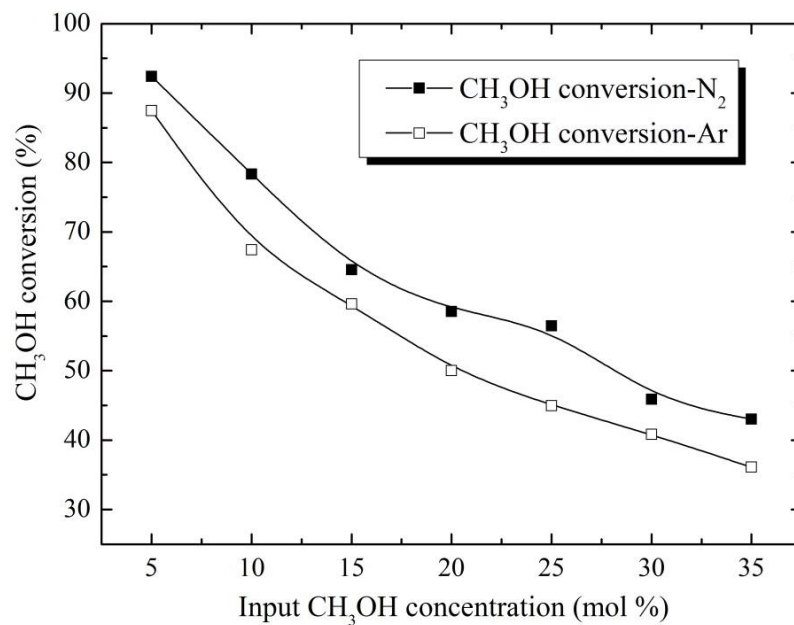


**Fig. 3 – Effect of input  $CH_3OH$  concentration on  $CH_3OH$  conversion**

Fig. 4 shows the influence of the  $CH_3OH$  concentration on the selectivity of  $H_2$  and CO and the

$H_2/CO$  molar ratio. The selectivity of  $H_2$  and  $CO$  produced in the  $CH_3OH/N_2$  RGA is significantly higher than that in the  $CH_3OH/Ar$  plasma, especially at a high methanol concentration ( $> 20\%$ ). The effect of the  $CH_3OH$  concentration on the selectivity of  $H_2$  and  $CO$  shows a similar evolution in both plasma chemical processes: the selectivity of syngas increases almost linearly as the  $CH_3OH$  concentration initially increases from 5 to 15 %, and then plateaus to an almost constant value when further increasing the methanol concentration.

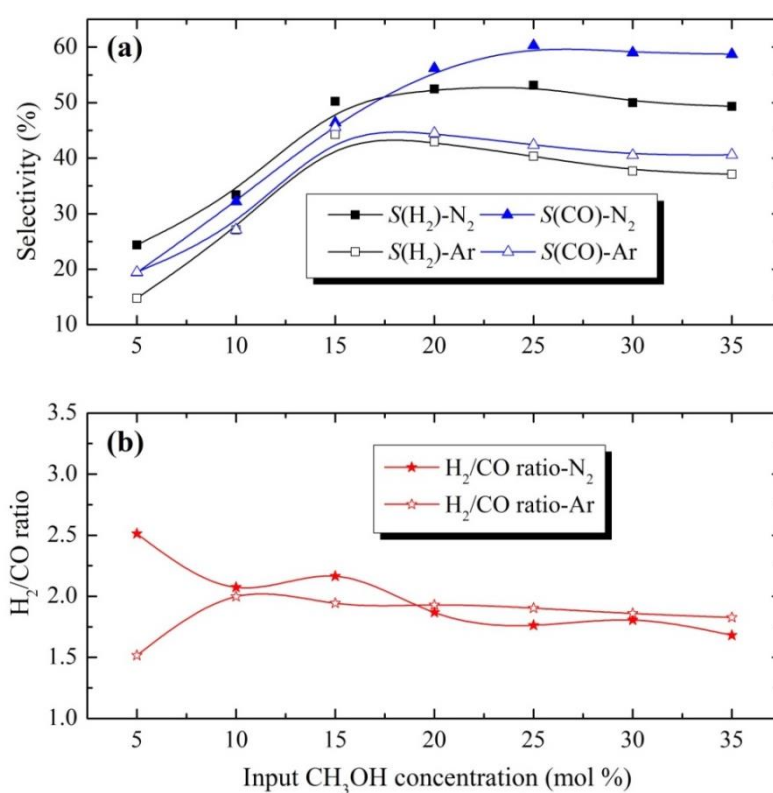


**Fig. 4 – Effect of input  $CH_3OH$  concentration on (a)  $H_2$  selectivity and  $CO$  selectivity; and (b)  $H_2/CO$  molar ratio**

It is expected that N-containing products (e.g.,  $NH_3$  and  $HCN$ ) were produced in the plasma methanol decomposition process in the  $CH_3OH/N_2$  plasma, as evidenced from the present of  $NH$  and  $CN$  bands in the emission spectra of the  $CH_3OH/N_2$  plasma.

From the stoichiometry of methanol decomposition reaction, a  $H_2/CO$  molar ratio of 2 would

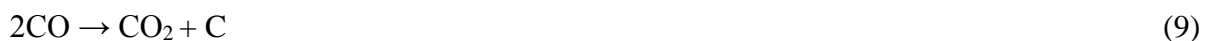
be expected. In this study, the H<sub>2</sub>/CO ratio is slightly below 2 for most operating conditions. We can see that increasing the CH<sub>3</sub>OH concentration from 5 to 10% leads to a noticeable drop of the H<sub>2</sub>/CO ratio from 2.51 to 2.07 in the CH<sub>3</sub>OH/N<sub>2</sub> plasma, while the H<sub>2</sub>/CO molar ratio in the CH<sub>3</sub>OH/Ar RGA increases from 1.52 to 2.00. This might be attributed to the formation of different byproducts in both plasma systems. As the methanol concentration increases from 10% to 35%, the H<sub>2</sub>/CO molar ratio in the CH<sub>3</sub>OH/N<sub>2</sub> plasma slightly decreases, whilst this parameter in the CH<sub>3</sub>OH/Ar plasma is almost constant.

Fig. 5 shows the effect of CH<sub>3</sub>OH concentration on the selectivities of gaseous byproducts. The selectivity of the gas products (CO<sub>2</sub>, CH<sub>4</sub>, C<sub>2</sub>H<sub>2</sub>, and C<sub>2</sub>H<sub>4</sub>) in the CH<sub>3</sub>OH/N<sub>2</sub> plasma decreases in the order: CH<sub>4</sub> > C<sub>2</sub>H<sub>2</sub> > C<sub>2</sub>H<sub>4</sub> ≈ CO<sub>2</sub>, whilst in the CH<sub>3</sub>OH/Ar gliding arc, the selectivity of these gases follows the order CO<sub>2</sub> > CH<sub>4</sub> > C<sub>2</sub>H<sub>2</sub> > C<sub>2</sub>H<sub>4</sub>. CO<sub>2</sub> was formed with significantly higher selectivity in the CH<sub>3</sub>OH/Ar RGA compared to the CH<sub>3</sub>OH/N<sub>2</sub> plasma. Increasing the concentration of CH<sub>3</sub>OH from 5 to 35% significantly decreases the CO<sub>2</sub> selectivity from 46.30 to 1.15% in the CH<sub>3</sub>OH/Ar plasma. In contrast, the selectivity of CO<sub>2</sub> is almost independent on the input concentration of CH<sub>3</sub>OH in the CH<sub>3</sub>OH/N<sub>2</sub> plasma and remains low (0.2%).

In the plasma methanol conversion process, CO<sub>2</sub> is more likely to be formed from the reaction of CO with OH radicals (Eq. (8)) [7].



Strong OH bands were observed in the spectra of the CH<sub>3</sub>OH/Ar plasma, whereas no OH bands were detected in the spectra of the CH<sub>3</sub>OH/N<sub>2</sub> RGA (see Fig. 9 and Fig. 10), which suggests that more CO<sub>2</sub> could be produced via Eq. (8) when Ar is used as a carrier gas, leading to a higher CO<sub>2</sub> selectivity. In addition, CO<sub>2</sub> could also be formed from the Boudouard reaction of CO:



Very low selectivity of  $\text{CO}_2$  (0.2%) was obtained in the  $\text{CH}_3\text{OH}/\text{N}_2$  RGA, which reveals that this reaction (Eq. (9)) might be inhibited in the plasma methanol conversion process using  $\text{N}_2$  as a carrier gas.

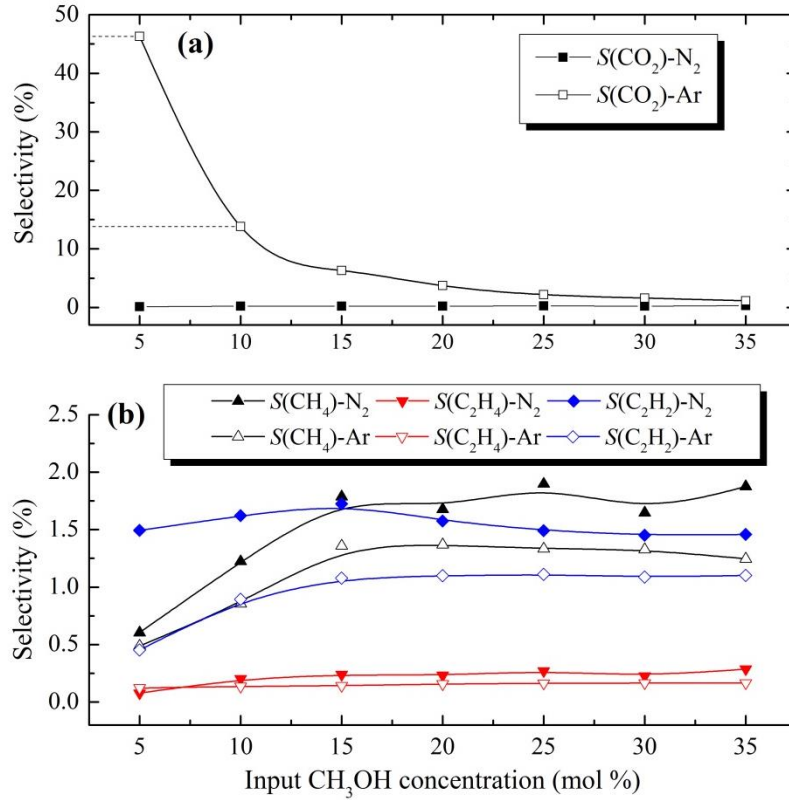


**Fig. 5 – Effect of input  $\text{CH}_3\text{OH}$  concentration on the selectivity of gaseous byproducts (a)  $\text{CO}_2$ , (b)  $\text{CH}_4$ ,  $\text{C}_2\text{H}_2$ , and  $\text{C}_2\text{H}_4$**

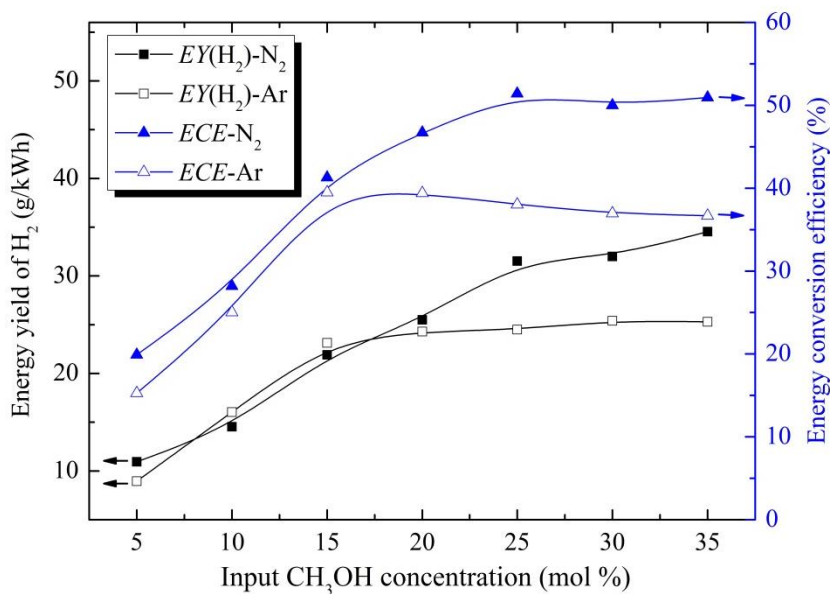


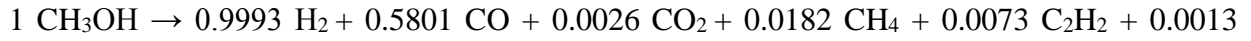
**Fig. 6 – Effect of input CH<sub>3</sub>OH concentration on energy conversion efficiency and energy yield of H<sub>2</sub>**

The effect of CH<sub>3</sub>OH concentration on the energy conversion efficiency and energy yield of H<sub>2</sub> is presented in Fig. 6. Both parameters follow the similar evolution of the selectivity of H<sub>2</sub> and CO with the increase of the CH<sub>3</sub>OH concentration (Fig. 4). At a CH<sub>3</sub>OH concentration of higher than 20%, both the energy conversion efficiency and energy yield of H<sub>2</sub> are higher in the CH<sub>3</sub>OH/N<sub>2</sub> RGA than those in the CH<sub>3</sub>OH/Ar RGA.

We find that the selectivities of gas products are almost constant as the methanol concentration varies between 15% and 35%, except the CO<sub>2</sub> selectivity in the argon plasma process, as shown in Figs. 4 and 5. This phenomenon suggests that there might be no significant changes of the dominant reaction routes in the plasma methanol conversion process. Fig. 7 shows the production of gaseous products increases linearly with increasing the converted methanol at the CH<sub>3</sub>OH concentration of 15-35% in the CH<sub>3</sub>OH/N<sub>2</sub> plasma. Similar evolution behavior of the gas products (except CO<sub>2</sub>) can be found in the Ar plasma-assisted methanol conversion process (Fig. 8). Note that the CO<sub>2</sub> formation decreases linearly with increasing the methanol converted, indicating that there is a

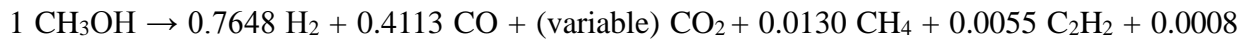
significant change in the formation of CO<sub>2</sub>. Both reactions can be globally represented by

*CH<sub>3</sub>OH/N<sub>2</sub> RGA plasma*



(10)

*CH<sub>3</sub>OH/N<sub>2</sub> RGA plasma*



(11)

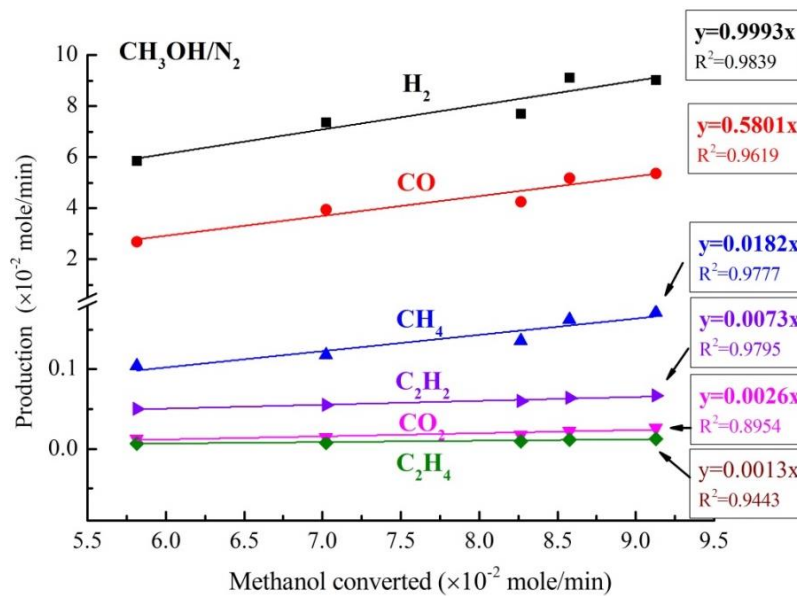


**Fig. 7 – Production of gaseous products as a function of methanol converted in the CH<sub>3</sub>OH/N<sub>2</sub> RGA at the CH<sub>3</sub>OH concentration of 15-35%**

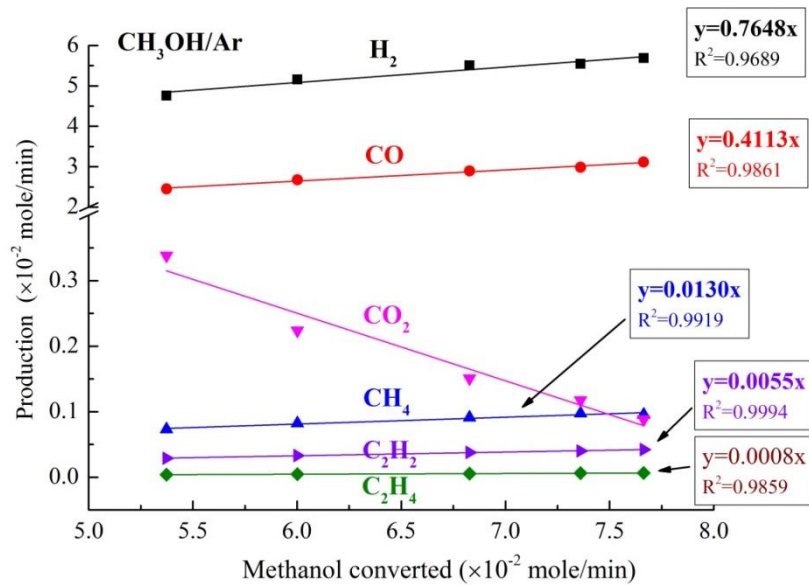


**Fig. 8 – Production of gaseous products as a function of methanol converted in the CH<sub>3</sub>OH/Ar RGA at the CH<sub>3</sub>OH concentration of 15-35%**

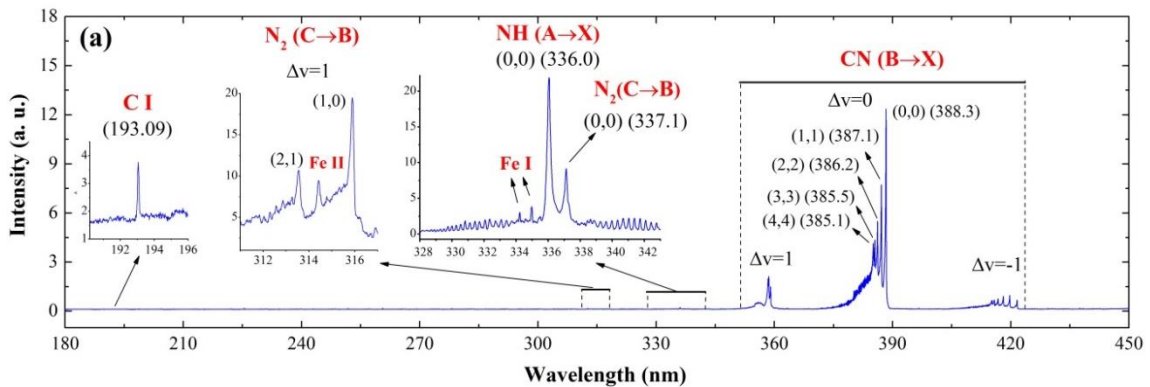
### 3.2 Optical diagnostics of plasma chemical processes

Optical emission diagnostics has been carried out to understand the formation of reactive species and to give new insights into the possible reaction mechanisms in the plasma methanol conversion processes. Fig. 9 shows typical emission spectra of the CH<sub>3</sub>OH/N<sub>2</sub> RGA. The spectra are clearly dominated by numerous strong CN ( $B^2\Sigma \rightarrow X^2\Sigma$ ,  $\Delta v = 1, 0, -1$ ) violet bands at an exposure time of 500  $\mu$ s. In addition, C I line (193.09 nm), N<sub>2</sub> second positive system ( $C^3\Pi_u \rightarrow B^3\Pi_g$ ), NH ( $A^3\Pi \rightarrow X^3\Sigma$ ) at 336.0 nm, C<sub>2</sub> swan system ( $d^3\Pi_g \rightarrow a^3\Pi_u$ ,  $\Delta v = 1, 0$ ), and CN violet system of  $\Delta v = -2$  can be observed using a long exposure time of 25 ms, as plotted in Fig. 9.

Different emission spectra were detected in the CH<sub>3</sub>OH/Ar plasma (Fig. 10) to those in the CH<sub>3</sub>OH/N<sub>2</sub> RGA. Besides the CN bands due to gas impurity, numerous C<sub>2</sub> swan bands ( $\Delta v = 1, 0, -1$ ) and weak CO fourth positive system ( $A^1\Pi \rightarrow X^1\Sigma$ ,  $\Delta v = 6-10$ ) can be observed. In addition, OH ( $A^2\Sigma^+ \rightarrow X^2\Pi$ ,  $\Delta v = 0$ ) and CH ( $A^2\Delta \rightarrow X^2\Pi$ ,  $\Delta v = 0$ ) bands, as well as H Balmer lines ( $H_\alpha$ ,  $H_\beta$ , and  $H_\delta$ ) can be clearly seen in the spectra. In contrast, these bands (OH, CH, and C<sub>2</sub>) and H atomic lines cannot be found in the spectra of the CH<sub>3</sub>OH/N<sub>2</sub> RGA. C I spectral lines at 193.09 nm and

247.87 nm, together with numerous argon atomic lines are also visible in the CH<sub>3</sub>OH/Ar plasma. Fe spectra lines from the electrode materials are detected in both plasma systems. An overview of these atomic lines and molecular bands that detected in the CH<sub>3</sub>OH/N<sub>2</sub> and CH<sub>3</sub>OH/Ar plasmas is presented in Table 1.

Vibrational temperature represents the chemical reactivity of vibrational excited species, and provides insight into the relative rates of vibration-vibration and vibration-translation energy exchange processes [28]. The vibrational temperature of CN in the CH<sub>3</sub>OH/N<sub>2</sub> RGA was determined from a group of CN ( $B^2\Sigma \rightarrow X^2\Sigma$ ,  $\Delta v=0$ ) violet bands using a Boltzmann plot [29]. The results show that increasing the input concentration of CH<sub>3</sub>OH from 5 to 35% results in a quasi-linear drop of the vibrational temperature from  $14300 \pm 800$  K to  $8930 \pm 1300$  K in the CH<sub>3</sub>OH/N<sub>2</sub> plasma, since CH<sub>3</sub>OH could quench the vibrational levels of CN [30]. It is interesting to note that the vibrational temperature in the CH<sub>3</sub>OH/N<sub>2</sub> plasma is considerably higher than that of other typical non-thermal plasmas, such as DBD in N<sub>2</sub> or Ar (2000-5000 K) [31-34] and glow discharge in N<sub>2</sub> (2000-4000 K) [35]. In addition, the vibrational temperature in the CH<sub>3</sub>OH/N<sub>2</sub> RGA plasma is also found higher than that of a pure N<sub>2</sub> RGA plasma (4000 K) [36] and an air/water gliding arc with knife-shaped electrodes (3900-4500 K) [37], showing higher vibrational levels of





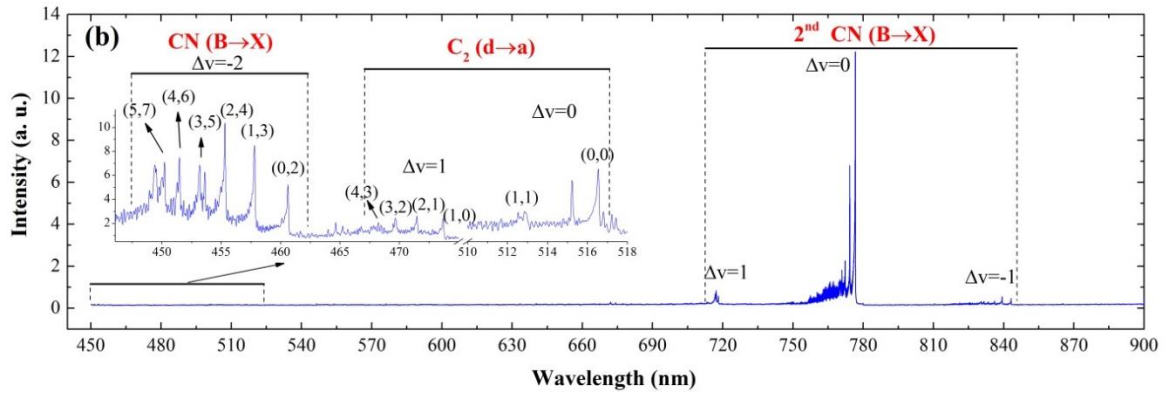


**Fig. 9** – Typical emission spectra of the CH<sub>3</sub>OH/N<sub>2</sub> plasma (CH<sub>3</sub>OH concentration= 5%, exposure time= 500 μs; for enlarged area: exposure time= 25 ms)

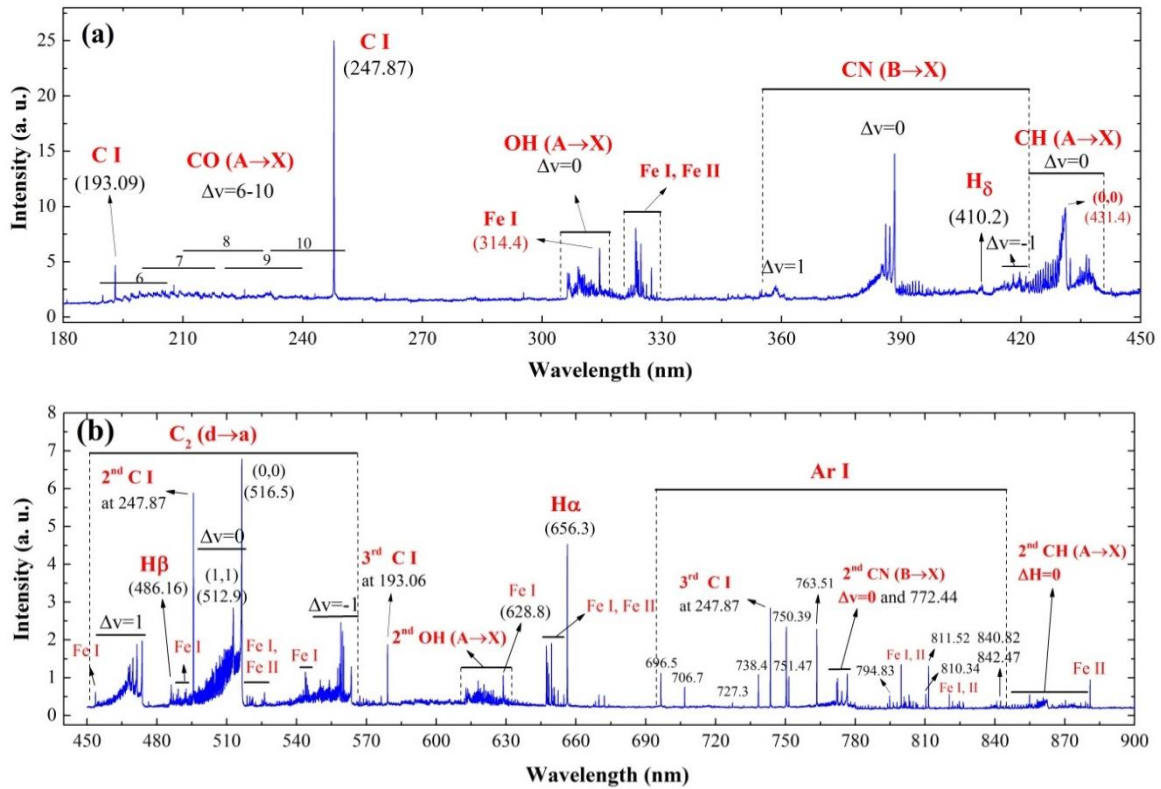


**Fig. 10** – Typical emission spectra of the CH<sub>3</sub>OH/Ar plasma (CH<sub>3</sub>OH concentration= 5%, exposure time= 25 ms)

Table 1 – Overview of the atomic lines and molecular bands in the spectra of the CH<sub>3</sub>OH/N<sub>2</sub> and

CH<sub>3</sub>OH/Ar plasmas

Species	Transition	Wavelength (nm)	
		CH <sub>3</sub> OH/N <sub>2</sub>	CH <sub>3</sub> OH/Ar
CI	2s <sup>2</sup> 2p <sup>2</sup> →2s <sup>2</sup> 2p3s	193.09	193.09, 247.87

N <sub>2</sub>	$C^3\Pi_u \rightarrow B^3\Pi_g$ (2, 1), (1, 0), (0, 0)		312-316, 337.1	ND <sup>a</sup>
NH	$A^3\Pi \rightarrow X^3\Sigma, (0, 0)$		336.0	ND
CN	$B^2\Sigma \rightarrow X^2\Sigma$	$\Delta v = 1, 0, -1$	355-360, 376-389, 410-420 2 <sup>nd</sup> order: 715-718.5, 756-777, 808-844	355-360, 376-389, 410-420
		$\Delta v = -2$	444-461	ND
C <sub>2</sub>	$d^3\Pi_g \rightarrow a^3\Pi_u$	$\Delta v = 1, 0$	464-474, 512-517	464-474, 512-517
		$\Delta v = -1$	ND	546-564
CO	$A^1\Pi \rightarrow X^1\Sigma, \Delta v = 6-10$		ND	190-250
OH	$A^2\Sigma^+ \rightarrow X^2\Pi, \Delta v = 0$		ND	306-320, 2 <sup>nd</sup> order: 611-640
H	Balmer system	$\delta$	ND	410.2
		$\beta$	ND	486.16
		$\alpha$	ND	656.3
CH	$A^2\Delta \rightarrow X^2\Pi, \Delta v = 0$		ND	421-440 2 <sup>nd</sup> order: 835-880
Ar	-		ND	695-844
Fe	-		314.43, 334.23, 334.98	314.4, 628.8, 647-655, 795-810, 820-827, 880.9

<sup>a</sup> ND: Not detected

the RGA CH<sub>3</sub>OH/N<sub>2</sub> plasma. The vibrational temperature of CN in the CH<sub>3</sub>OH/Ar plasma was also obtained using the aforementioned method by adding 5 mol % N<sub>2</sub> into the CH<sub>3</sub>OH/Ar plasma, and the corresponding vibrational temperature is in the range of 6600 ± 900 to 8100 ± 400 K, which is also much lower than that in the CH<sub>3</sub>OH/N<sub>2</sub> plasma.

The electron density of the CH<sub>3</sub>OH/Ar plasma can be determined from the Stark broadening of the Ar atomic line at 696.5 nm. The detailed method can be found in previous works [38, 39]. The estimated electron density of the 5% CH<sub>3</sub>OH/Ar RGA is (1.53 ± 0.14) × 10<sup>16</sup> cm<sup>-3</sup>. This value is about an order of magnitude lower than that of the AC gliding arc with knife-shaped electrodes [11].

In this study, the electron density obtained in the CH<sub>3</sub>OH/Ar and CH<sub>3</sub>OH/N<sub>2</sub> RGA plasmas is significantly higher (several orders of magnitude) than that of typical non-thermal plasmas, such as DBD (10<sup>10</sup>-10<sup>13</sup> cm<sup>-3</sup>) and corona discharge (10<sup>9</sup>-10<sup>13</sup> cm<sup>-3</sup>) [11, 40].

### 3.3 Reaction Mechanisms

The possible dominant reaction pathways in the RGA decomposition of methanol are schematically shown in Fig. 11. At a high concentration of CH<sub>3</sub>OH (e.g., 20-35%), electron impact dissociation of methanol via different reaction channels (Eq. (12)-(18)) plays a dominant role in the decomposition of CH<sub>3</sub>OH into a variety of radicals or intermediates [41-43], with subsequent radical recombination reactions to form higher hydrocarbons or further dissociation of radicals and intermediates [25].



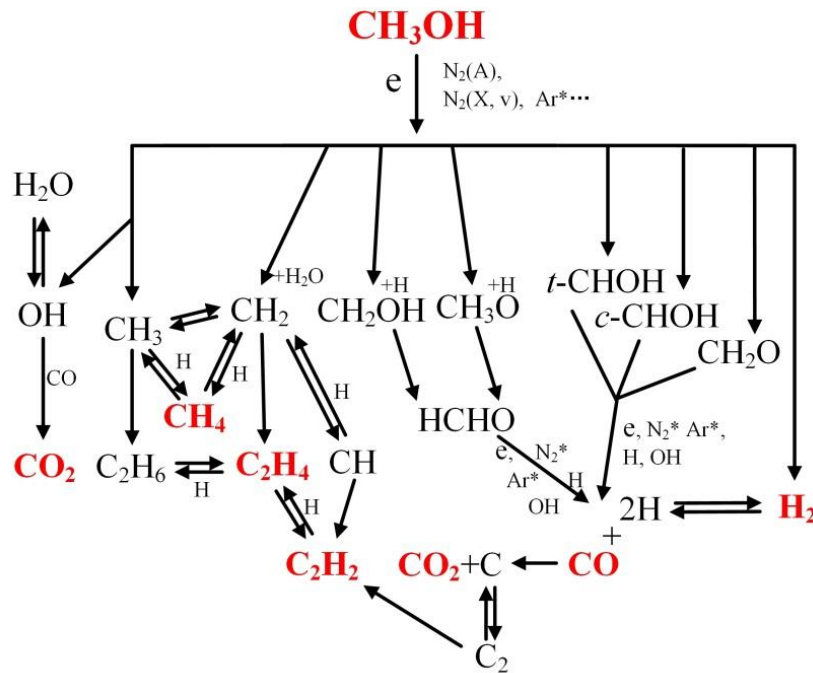
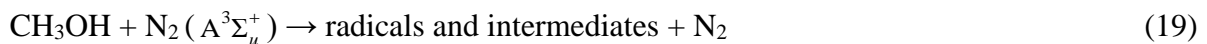


**Fig. 11 – Possible reaction pathways of methanol decomposition in  $\text{CH}_3\text{OH}/\text{N}_2$  and  $\text{CH}_3\text{OH}/\text{Ar}$  gliding arc plasmas**

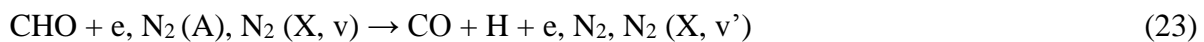
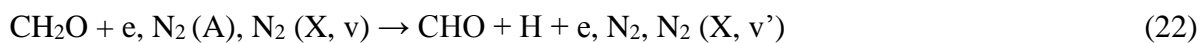
In the  $\text{CH}_3\text{OH}/\text{N}_2$  and  $\text{CH}_3\text{OH}/\text{Ar}$  gliding arc plasmas, initially formed highly energetic electrons interact with the carrier gas ( $\text{N}_2$  or  $\text{Ar}$ ) to produce a cascade of processes yielding a variety of chemically reactive species including electronically excited metastable  $\text{N}_2(\text{A}^3\Sigma_u^+)$ , vibrationally excited  $\text{N}_2(\text{X}^2\Sigma_g^+, \nu)$ , and electronically excited  $\text{Ar}^*$  species [44-47]. These excited species are believed to make a significant contribution to the dissociation of methanol (Eq. (19)-(21)) into a variety of radicals and intermediates (e.g.,  $\text{CH}_3$ ,  $\text{OH}$ ,  $\text{CH}_2\text{O}$ ,  $\text{CH}_2\text{OH}$ ), especially at a low concentration of methanol (e.g., 5%) [44, 45].



Previous plasma modeling work has demonstrated that quenching reactions with metastable nitrogen  $\text{N}_2(\text{A}^3\Sigma_u^+)$  appear to be important in the destruction of ethylene (10-10000 ppm) besides the reactions with radicals in an atmospheric pressure air DBD, while the direct electron impact

dissociation reactions are negligible for the destruction of ethylene [47]. Diamy et al. have also shown that metastable  $N_2$  species are critical in the initial decomposition of methane in a  $CH_4/N_2$  glow discharge [30, 48]. In addition, Pintassilgo et al. have demonstrated that the vibrational excited  $N_2$  could contribute much to the decomposition of  $CH_4$  in a 2%  $CH_4/N_2$  afterglow plasma [44, 45]. We can find that more reaction channels for the conversion of methanol exist in the  $CH_3OH/N_2$  plasma due to the formation of more excited species compared to the  $CH_3OH/Ar$  plasma, which can also explain the higher conversion of methanol obtained in the plasma reaction using  $N_2$  as a carrier gas.

$CH_2O$  is a key intermediate from the initial decomposition of methanol (Eq. (16)-(21)).  $CH_2O$  is unstable in non-thermal plasmas and can be further decomposed to form  $H_2$  and  $CO$  through the dissociation with electrons and excited species (e.g.,  $N_2(A^3\Sigma_u^+)$ ,  $N_2(X^2\Sigma_g^+, \nu)$ ,  $Ar^*$ ),



$H_2$  can also be generated from the direct dissociation of methanol (e.g., Eq. 16-21) or the recombination of  $H$  radicals from methanol decomposition (e.g., Eq. (24)).

In addition, the  $H$  and  $OH$  radicals that present in the plasma bulk may also contribute to the conversion of  $CH_2O$  and  $CHO$  through the following reactions, generating  $CO$ ,  $H_2$ , and  $H_2O$  [49].



Very low selectivities of hydrocarbons (mainly  $CH_4$ ,  $C_2H_2$  and  $C_2H_4$ ) have been obtained in the

CH<sub>3</sub>OH/N<sub>2</sub> (2.7-3.8%) and CH<sub>3</sub>OH/Ar (1.1-2.6%) plasmas. The initially generated CH<sub>3</sub> and CH<sub>2</sub> radicals are the key species to form these hydrocarbons (CH<sub>4</sub>, C<sub>2</sub>H<sub>2</sub>, and C<sub>2</sub>H<sub>4</sub>) through further dissociation or recombination reactions. For instance, CH<sub>4</sub> can be formed from the recombination of CH<sub>3</sub> and H, which can explain why the selectivity of CH<sub>4</sub> is one order of magnitude higher than that of C<sub>2</sub> hydrocarbons.

Carbon can be mainly formed from the Boudouard reaction (Eq. (9)), which also leads to the formation of CO<sub>2</sub>. CO<sub>2</sub> might also be formed via water gas shift reaction (Eq. (29)).



### 3.4 Comparison of different plasma technologies for hydrogen production from methanol

Table 2 shows a comparison of the performance (e.g., methanol conversion rate, selectivity of syngas, and energy yield of H<sub>2</sub>) of plasma methanol conversion using different processes and plasma systems.

In the steam reforming of methanol using a pulsed gliding arc reactor, a high energy yield of H<sub>2</sub> was achieved with a relatively low conversion of methanol [3]. [Note the energy cost for the production of steam has not been considered in the calculation of energy yield of H<sub>2</sub>.](#) The combination of plasma with catalysts (e.g., Cu/Al<sub>2</sub>O<sub>3</sub> and Cu/ZnO) was also used to enhance the conversion of CH<sub>3</sub>OH in the steam reforming of methanol by a DBD [13, 24]. [However, the energy efficiency of the plasma-catalytic process is much lower in a DBD plasma reactor compared to that using a gliding arc.](#)

**Table 2 – Comparison of the performance of RGA plasmas with other non-thermal plasmas for hydrogen production from methanol conversion**

Plasma type	Process	Carrier gas	Reactants	Power supply/ Discharge power	CH <sub>3</sub> OH conversion (%)	S(H <sub>2</sub> ) (%)	S(CO) (%)	H <sub>2</sub> /CO	EY(H <sub>2</sub> ) <sup>c</sup> (g/kWh)	Ref.
Pulsed GAD	SR <sup>a</sup>	Ar 2 l/min	H <sub>2</sub> O + 5-85% CH <sub>3</sub> OH: 2-20 ml/min	AC, 250 Hz, 25 kV, 0.3-0.45W	3-33	-	-	-	~50- 176	[3]
DBD + Cu/Al <sub>2</sub> O catalyst	SR	Ar 10 ml/min	H <sub>2</sub> O+50 % CH <sub>3</sub> OH; CH <sub>3</sub> OH: 0.0165 ml/min	AC, 18.5 kHz ~12.5-21.5 W	15-80	~16- 45	-	-	~0.5-16	[13]
DBD + Cu/ZnO catalyst	SR	N <sub>2</sub>	H <sub>2</sub> O + 50 % CH <sub>3</sub> OH; CH <sub>3</sub> OH: 0.008 ml/min	AC, 50 kHz, 0-4 kV, 0.12-0.47 W	6-54.4	-	~3-14	-	-	[24]
MHCD	DEC <sup>b</sup>	N <sub>2</sub> 10.5-23.7 ml/min	4.7-56.7% CH <sub>3</sub> OH	DC, ~0.8-1.3 W	7.4-47.0	55- 80	50- 80	1.5- 2.8	1.2-10.8	[2]
GAD	DEC	Ar 43.3-86.6 ml/min	17.4-37.8% CH <sub>3</sub> OH	AC, < 300W	51.8-62.2	43.4- 49.5	81.4- 81.9	1.14- 1.2	~6.9	[4]
Corona	DEC	Ar 40 ml/min	20-75% CH <sub>3</sub> OH	AC, 2 kHz 0.8 kV, 12 W	10-80	-	-	-	~4.5	[22]
DBD	DEC	N <sub>2</sub> 100 ml/min	1% CH <sub>3</sub> OH	AC, 50 Hz, 0.21-1.99 W	8-26	12- 21.7	11.7- 20.0	1.96- 2.70	~0.05- 0.63	[15]
RGA	DEC	Ar 7.9-11.5 l/min	5-35% CH <sub>3</sub> OH	DC, 10 kV, 105.2-271.6 W	36.1-87.5	14.8- 44.3	19.5- 45.6	1.52- 2.00	8.95- 25.40	This work
		N <sub>2</sub> 8.8-12.8 l/min		DC, 10 kV, 149.8-349.4 W	43.0-92.4	24.4- 53.1	19.4- 60.3	1.76- 2.51	10.94- 34.54	

<sup>a</sup> SR: Steam reforming of methanol

<sup>b</sup> DEC: Non-oxidative decomposition of methanol

<sup>c</sup> The energy yield of H<sub>2</sub> (1 g/kWh) corresponds to the energy cost of 31.67 kJ/mol H<sub>2</sub>

In Table 2, we can see that non-oxidative decomposition of methanol offers relatively higher selectivities of H<sub>2</sub> and CO, as well as higher H<sub>2</sub>/CO molar ratio, compared with steam reforming of methanol processes due to limited water gas shift reaction. Compared to other plasma systems (e.g.

DBD), the RGA plasma shows a significantly higher conversion of methanol, a relatively high selectivity of syngas, and a highest energy yield of hydrogen in plasma decomposition of methanol process. It is also interesting to note that the RGA plasmas can provide a feed flow rate, or processing capacity, of several orders of magnitude higher (e.g., 7.9-11.5 l/min) than that using other non-thermal plasma systems (e.g., 10.5-100 ml/min in a DBD reactor), whilst allowing for the conversion of a wider range of reactant concentration, both of which are beneficial to the industrial applications.

#### 4. Conclusions

In this study, non-oxidative decomposition of methanol for hydrogen production has been carried out in the atmospheric pressure DC rotating gliding arc plasma reactor. The effect of carrier gas and input CH<sub>3</sub>OH concentration on the reaction performance of the plasma conversion processes has been evaluated. The use of N<sub>2</sub> as a carrier gas in the plasma methanol conversion shows much better performance compared with the CH<sub>3</sub>OH/Ar gliding arc in terms of the CH<sub>3</sub>OH conversion, syngas selectivity, energy yield of H<sub>2</sub>, and energy conversion efficiency of the plasma process. It is found that increasing the input methanol concentration from 5 to 35 % significantly decreases the CH<sub>3</sub>OH conversion from 92.4 to 43.0 % in the CH<sub>3</sub>OH/N<sub>2</sub> RGA and from 87.5 to 36.1 % in the CH<sub>3</sub>OH/Ar RGA. Optical emission diagnostics of the plasma process clearly shows the generation of a variety of reactive species in both plasmas. The estimated electron density of the 5% CH<sub>3</sub>OH/Ar plasmas is  $(1.53 \pm 0.14) \times 10^{16} \text{ cm}^{-3}$ , which is significantly higher than that of other typical non-thermal plasmas, such as DBD ( $10^{10}$ - $10^{13} \text{ cm}^{-3}$ ) and corona discharges ( $10^9$ - $10^{13} \text{ cm}^{-3}$ ), indicating a high processing capacity of the RGA plasma. The vibrational and electronically excited species (e.g., N<sub>2</sub>



( $A^3\Sigma_u^+$ ),  $N_2(X^2\Sigma_g^+, \nu)$ ,  $Ar^*$ ) are expected to play an important role in the methanol decomposition process. we find that the RGA plasma can provide a feed flow rate, or processing capacity, of several orders of magnitude higher (e.g., 7.9-11.5 l/min) than that using other non-thermal plasma systems (e.g., 10.5-100 ml/min in a DBD reactor), whilst allowing for the conversion of a wider range of reactant concentration, both of which are beneficial to the industrial applications.

## Acknowledgement

The support of this work by the Specialized Research Fund for the Doctoral Program of Higher Education of China (20120101110099), the Fundamental Research Funds for the Central Universities (2014FZA4011) and the UK EPSRC Bioenergy Challenge Programme (EP/M013162/1) is gratefully acknowledged. H. Zhang acknowledges the support by Lin Guangzhao & Hu Guozan Graduate Education International Exchange Fund.

## References

- [1] Chen SH, Chen HL, Lee HM, Chao Y. and Chang MB. Review of plasma catalysis on hydrocarbon reforming for hydrogen production—Interaction, integration, and prospects. *Appl Catal B* 2008, 85(1): 1-9.
- [2] Lindner PJ and Besser RS. Hydrogen production by methanol reforming in a non-thermal atmospheric pressure microplasma reactor. *Int J Hydrogen Energy* 2012, 37(18): 13338-49.
- [3] Burlica R, Shih K, Hnatiuc B, and Locke BR. Hydrogen generation by pulsed gliding arc discharge plasma with sprays of alcohol solutions. *Ind Eng Chem Res* 2011, 50(15): 9466-70.
- [4] LÜ Y, Yan W, Hu S, and WANG B. Hydrogen production by methanol decomposition using gliding arc gas discharge. *J Fuel Chem. Technol* 2012, 40(6): 698-706.
- [5] Henriques J, Bundaleska N, Tatarova E, Dias FM, and Ferreira CM. Microwave plasma torches driven by surface wave applied for hydrogen production. *Int J Hydrogen Energy* 2011, 36(1): 345-54.
- [6] Durka T, Stefanidis GD, Van Gerven T, and Stankiewicz AI. Microwave-activated methanol steam reforming for hydrogen production. *Int J Hydrogen Energy* 2011, 36(20): 12843-52.
- [7] Bundaleska N, Tsyganov D, Saavedra R, Tatarova E, Dias FM, and Ferreira CM. Hydrogen production from methanol reforming in microwave "tornado" type plasma. *Int J Hydrogen Energy* 2013, 38(22): 9145-57.
- [8] Wang Y, You Y, Tsai C, and Wang L. Production of hydrogen by plasma-reforming of methanol. *Int J*

Hydrogen Energy 2010, 35(18): 9637-40.

- [9] Geissler K, Newson E, Vogel F, Truong T, Hottinger P, and Wokaun A. Autothermal methanol reforming for hydrogen production in fuel cell applications. *Phys Chem Chem Phys* 2001, 3(3): 289-93.
- [10] Sá S, Silva H, Brandão L, Sousa JM, and Mendes A. Catalysts for methanol steam reforming—A review. *Appl Catal B* 2010, 99(1): 43-57.
- [11] Tu X and Whitehead JC. Plasma dry reforming of methane in an atmospheric pressure AC gliding arc discharge: Co-generation of syngas and carbon nanomaterials. *Int J Hydrogen Energy* 2014, 39(18): 9658-69.
- [12] Liu SY, Mei DH, Shen Z, and Tu X. Nonoxidative Conversion of Methane in a Dielectric Barrier Discharge Reactor: Prediction of Reaction Performance Based on Neural Network Model. *J Phys Chem C* 2014, 118(20): 10686-93.
- [13] Ge W, Duan X, Li Y, and Wang B. Plasma-catalyst synergy during methanol steam reforming in dielectric barrier discharge micro-plasma reactors for hydrogen production. *Plasma Chem Plasma Process* 2015, 35(1): 187-99.
- [14] Kalra CS, Cho YI, Gutsol A, Fridman A and Rufael TS. Gliding arc in tornado using a reverse vortex flow. *Rev Sci Instrum* 2005, 71(2): 25110.
- [15] Futamura S and Kabashima H. Effects of reactor type and voltage properties in methanol reforming with nonthermal plasma. *IEEE Trans Ind Appl* 2004, 40(6): 1459-66.
- [16] Bo Z, Yan JH, Li XD, Chi Y, and Cen KF. Plasma assisted dry methane reforming using gliding arc gas discharge: Effect of feed gases proportion. *Int J Hydrogen Energy* 2008, 33(20): 5545-53.
- [17] Fridman A, Nester S, Kennedy LA, Saveliev A, and Mutaf-Yardimci O. Gliding arc gas discharge. *Prog Energy Combust Sci* 1999, 25(2): 211-31.
- [18] Tu X, Gallon HJ, and Whitehead JC. Dynamic behavior of an atmospheric argon gliding arc plasma. *IEEE Tran Plasma Sci* 2011, 39(11): 2900-1.
- [19] Zhang H., Du CM, Wu AJ, Bo Z, Yan, JH, and Li XD. Rotating gliding arc assisted methane decomposition in nitrogen for hydrogen production. *Int J Hydrogen Energy* 2014, 39(24): 12620-35.
- [20] Bromberg L, Cohn DR, Rabinovich A, and Alexeev N. Plasma catalytic reforming of methane. *Int J Hydrogen Energy* 1999, 24(12): 1131-7.
- [21] Indarto A, Choi J, Lee H, and Song HK. Effect of additive gases on methane conversion using gliding arc discharge. *Energy* 2006, 31(14): 2986-95.
- [22] Li H, Zou J, Zhang Y, and Liu C. Novel plasma methanol decomposition to hydrogen using corona discharges. *Chem Lett* 2004, 33(6): 744-745.
- [23] Lee DH and Kim T. Plasma-catalyst hybrid methanol-steam reforming for hydrogen production. *Int J Hydrogen Energy* 2013, 38(14): 6039-43.
- [24] Kim T, Jo S, Song Y, and Lee DH. Synergetic mechanism of methanol-steam reforming reaction in a catalytic reactor with electric discharges. *Appl Energ* 2014, 113: 1692-9.
- [25] Tu X and Whitehead JC. Plasma-catalytic dry reforming of methane in an atmospheric dielectric barrier

- discharge: Understanding the synergistic effect at low temperature. *Appl Catal B* 2012, 125: 439-48.
- [26] Gallon HJ, Tu X, and Whitehead JC. Effects of reactor packing materials on H<sub>2</sub> production by CO<sub>2</sub> reforming of CH<sub>4</sub> in a dielectric barrier discharge. *Plasma Process Polym* 2012, 9(1): 90-7.
- [27] Yao S, Zhang X, and Lu B. Influence of plasma reactor structure on methanol oxidation. *Aiche J* 2005, 51(5): 1558-64.
- [28] Biloiu C, Sun X, Harvey Z, and Scime E. Determination of rotational and vibrational temperatures of a nitrogen helicon plasma. *Rev Sci. Instrum* 2006, 77 (10): 10F117.
- [29] Ogungbesan B, Kumar R, Su L, and Sassi M. Experimental validation of local thermal equilibrium in a MW plasma torch for hydrogen production. *Int J Hydrogen Energy* 2013, 38(35): 15210-8.
- [30] Legrand JC, Diamy AM, Hrach R, and Hrachova V. Methane Conversion in the Flowing Afterglow of a Dinitrogen Microwave Plasma: Initiation of the Reaction. *Contrib Plasma Phys* 1997, 37(6): 521-37.
- [31] Stanfield SA, Menart J, DeJoseph C, Kimmel RL, and Hayes JR. Rotational and vibrational temperature distributions for a dielectric barrier discharge in air. *Aiaa J* 2009, 47(5): 1107-15.
- [32] Zhang S, Wang W, Jia L, Liu Z, Yang Y, and Dai L. Rotational, vibrational, and excitation temperatures in bipolar nanosecond-pulsed diffuse dielectric-barrier-discharge plasma at atmospheric pressure. *IEEE Tran Plasma Sci* 2013, 41(2): 350-4.
- [33] Masoud N, Martus K, Figus M, and Becker K. Rotational and vibrational temperature measurements in a high-pressure cylindrical dielectric barrier discharge (C-DBD). *Contribution Plasma Phys* 2005, 45(1): 32-9.
- [34] Tu X, Gallon HJ, and Whitehead JC. Electrical and spectroscopic diagnostics of a single-stage plasma-catalysis system: effect of packing with TiO<sub>2</sub>. *J Phys D: Appl Phys* 2011, 44(48): 482003.
- [35] Staack D, Farouk B, Gutsol AF, and Fridman AA. Spectroscopic studies and rotational and vibrational temperature measurements of atmospheric pressure normal glow plasma discharges in air. *Plasma Sources Sci Technol*, 2006, 15(4): 818.
- [36] Wu AJ, Zhang H, Li XD, Lu SY, Du CM, and Yan JH. Determination of Spectroscopic Temperatures and Electron Density in Rotating Gliding Arc Discharge. *IEEE Tran Plasma Sci* 2015, 43(3): 836-45.
- [37] Tu X, Yu L, Yan JH, Cen KF, and Chéron BG. Dynamic and spectroscopic characteristics of atmospheric gliding arc in gas-liquid two-phase flow. *Phys Plasmas* 2009, 16(11): 113506.
- [38] Griem HR. *Plasma spectroscopy*. New York: McGraw-Hill; 1964.
- [39] Tu X, Chéron BG, Yan JH, and Cen KF. Electrical and spectroscopic diagnostic of an atmospheric double arc argon plasma jet. *Plasma Sources Sci Technol* 2007, 16(4): 803.
- [40] Tu X, Verheyde B, Corthals S, Paulussen S, and Sels BF. Effect of packing solid material on characteristics of helium dielectric barrier discharge at atmospheric pressure. *Phys Plasmas* 2011, 18(8): 80702.
- [41] Han Y, Wang J, Cheng D, and Liu C. Density functional theory study of methanol conversion via cold plasmas. *Ind Eng Chem Res* 2006, 45(10): 3460-7.
- [42] Chang A and Lin SH. A theoretical study of the O(<sup>1</sup>D) + CH<sub>4</sub> reaction I. *Chem Phys Lett* 2002, 363(1): 175-81.

- [43] Krasnoperov LN and Michael JV. High-temperature shock tube studies using multipass absorption: rate constant results for  $\text{OH} + \text{CH}_3$ ,  $\text{OH} + \text{CH}_2$ , and the dissociation of  $\text{CH}_3\text{OH}$ . *J Phys Chem A* 2004, 108(40): 8317-23.
- [44] Pintassilgo CD and Loureiro J. Kinetic study of a  $\text{N}_2\text{-CH}_4$  afterglow plasma for production of N-containing hydrocarbon species of Titan's atmosphere. *Adv Space Res* 2010, 46(5): 657-71.
- [45] Pintassilgo CD and Loureiro J. Production of hydrocarbons and nitriles using a  $\text{N}_2\text{-CH}_4$  afterglow plasma for simulation of Titan's atmosphere. *Planet Space Sci* 2009, 57(13): 1621-30.
- [46] Hsieh L, Lee W, Chen C, Chang M, and Chang H. Converting methane by using an RF plasma reactor. *Plasma Chem Plasma Process* 1998, 18(2): 215-39.
- [47] Aerts R, Tu X, De Bie C, Whitehead JC, and Bogaerts, A. An investigation into the dominant reactions for ethylene destruction in non-thermal atmospheric plasmas. *Plasma Process Polym* 2012, 9(10), 994-1000.
- [48] Damiy A, Hrach R, Hrachova V, and Legrand J. Influence of C atom concentration for acetylene production in a  $\text{CH}_4/\text{N}_2$  afterglow. *Vacuum* 2001, 61(2): 403-7.
- [49] Liu C, Mallinson R, and Lobban L. Nonoxidative methane conversion to acetylene over zeolite in a low temperature plasma. *J Catal* 1998, 179(1): 326-34.